Stabilization of cardiac ryanodine receptor prevents intracellular calcium leak and arrhythmias

Stephan E. Lehnart*, Cecile Terrenoire†, Steven Reiken*, Xander H. T. Wehrens*, Long-Sheng Song‡, Erik J. Tillman*, Salvatore Mancarella*, James Coromilas§, W. J. Lederer‡¶, Robert S. Kass†, and Andrew R. Marks*§‖

*Departments of Physiology and Cellular Biophysics, Clyde and Helen Wu Center for Molecular Cardiology, and Departments of †Pharmacology and §Medicine, College of Physicians and Surgeons, Columbia University, New York, NY 10032; ‡Medical Biotechnology Center, University of Maryland Biotechnology Institute, 725 West Lombard Street, Baltimore, MD 21201; and ¶Department of Physiology, University of Maryland, Baltimore, MD 21201

Contributed by Andrew R. Marks, March 15, 2006

Catecholaminergic polymorphic ventricular tachycardia is a form of exercise-induced sudden cardiac death that has been linked to mutations in the cardiac Ca^{2+} release channel/ryanodine receptor (RyR2) located on the sarcoplasmic reticulum (SR). We have shown that catecholaminergic polymorphic ventricular tachycardia-linked RyR2 mutations significantly decrease the binding affinity for calstabin-2 (FKBP12.6), a subunit that stabilizes the closed state of the channel. We have proposed that RyR2-mediated diastolic SR Ca^{2+} leak triggers ventricular tachycardia (VT) and sudden cardiac death. In calstabin-2-deficient mice, we have now documented diastolic SR Ca^{2+} leak, monophasic action potential alternans, and bidirectional VT. Calstabin-deficient cardiomyocytes exhibited SR Ca^{2+} leak-induced aberrant transient inward currents in diastole consistent with delayed after-depolarizations. The 1,4-benzothiazepine JTV519, which increases the binding affinity of calstabin-2 for RyR2, inhibited the diastolic SR Ca^{2+} leak, monophasic action potential alternans and triggered arrhythmias. Our data suggest that calstabin-2 deficiency is as a critical mediator of triggers that initiate cardiac arrhythmias.

calcium release channel | calstabin | heart failure | JTV519 | sudden cardiac death

Catecholaminergic polymorphic ventricular tachycardia (CPVT) is an inherited autosomal-dominant syndrome causing sudden cardiac death with mortality rates of up to 50% at 35 years (1, 2). CPVT has been linked to cardiac Ca^{2+} release channel/ryanodine receptor (RyR2) missense mutations. Symptomatic carriers of CPVT-linked RyR2 mutations have structurally normal hearts and typically present with syncope or sudden cardiac death due to stress-induced ventricular arrhythmias (1, 3). Stimulation of cardiac β-adrenergic receptors (β-ARs) can predispose to ventricular tachycardias (VTs) in CPVT mutation carriers, as evidenced by the fact that β-AR blockers provide only partial protection (4).

Heterologous expression of CPVT-mutant RyR2 channels in atrial tumor cells resulted in a significant intracellular Ca^{2+} leak during β-AR stimulation (5), whereas normal mouse cardiomyocytes did not show any significant Ca^{2+} leak under resting conditions during β-AR stimulation (6). We reported earlier that six distinct and structurally unrelated RyR2 missense mutations found in CPVT carriers all decrease the binding affinity of calstabin-2 for RyR2 (1, 7). This finding suggests a common mechanism for the RyR2 gain-of-function defect associated with exercise-induced arrhythmias (1, 7). *Calstabin-2*$^{-/-}$-deficient mice exhibited catecholaminergic VTs and delayed after-depolarizations (DADs) in isolated cardiomyocytes (7), indicating that intracellular Ca^{2+} leak may trigger membrane depolarizations that are responsible for exercise-induced arrhythmias (8–10) similar to those observed during digitalis-induced Ca^{2+} overload (11).

RyR2 are large (≈3 million Da) intracellular Ca^{2+} release channel macromolecular complexes comprised of four RyR2 monomers. Each RyR2 binds one calstabin-2 and signaling modules comprised of cAMP-activated protein kinase A (PKA) holoenzyme, the phosphatases PP1 and PP2A, the phosphodiesterase PDE4D3, and their respective targeting proteins (12, 27). Sympathetic nervous system activation results in PKA phosphorylation of RyR2 at Ser-2808, which significantly increases channel open probability (13, 14). CPVT-linked RyR2 mutations that result in depletion of calstabin-2 from the channel complex (1, 7) can be rescued *in vitro* and *in vivo* with a mutant calstabin-2-D37S that binds to PKA-phosphorylated RyR2 (7, 15). Pharmacologic treatment of haploinsufficient *calstabin-2*$^{+/-}$, but not of *calstabin-2*$^{-/-}$, knockout mice with JTV519, which increases calstabin-2 binding to RyR2, prevented cardiac arrhythmias, sudden cardiac death, and the progression of heart failure in relevant animal models (16, 17).

Because DADs and arrhythmia triggers occur in conjunction with diastolic sarcoplasmic reticulum (SR) Ca^{2+} leak in heart failure in which RyR2 are chronically depleted of calstabin-2 (18–21), and CPVT missense mutations decrease the calstabin-2 binding affinity to RyR2 (1, 7), we hypothesized that calstabin-2 depletion from the RyR2 complex during β-AR stimulation constitutes a common mechanism of arrhythmia initiation for catecholaminergic VT. We examined SR Ca^{2+} leak in a murine calstabin-2 deficiency model and investigated whether JTV519-induced rebinding of calstabin-2 to RyR2 could restore normal function and inhibit triggers of arrhythmias at the cellular level.

Results

JTV519-treated WT, haploinsufficient *calstabin-2*$^{+/-}$ and *calstabin-2*$^{-/-}$-deficient mice did not exhibit VT under resting conditions, in agreement with previous results (7, 16). Isoproterenol (ISO) (0.5 mg·kg^{-1} i.p.) produced a significant increase in maximal heart rate in all groups: WT, 750 ± 42 min^{-1}; *calstabin-2*$^{+/-}$, 748 ± 38 min^{-1}; or *calstabin-2*$^{-/-}$, 747 ± 44 min^{-1} (each $P < 0.05$ compared with baseline). JTV519 treatment (7-day continuous infusion of 0.5 mg·kg^{-1}·hr^{-1} via osmotic minipump) did not affect the increase in heart rate due to ISO: *calstabin-2*$^{+/-}$ plus JTV519, 732 ± 45 min^{-1}; or *calstabin-2*$^{-/-}$ plus JTV519, 728 ± 52 min^{-1} (each $P < 0.05$ compared with baseline).

WT, *calstabin-2*$^{+/-}$, and *calstabin-2*$^{-/-}$ mice underwent programmed electrical stimulation (PES) to test for arrhythmia susceptibility. Compared with untreated animals, JTV519-

Conflict of interest statement: A.R.M. is on the scientific advisory board and owns shares in ARMGO Pharma, Inc., a start-up company that is developing JTV519 derivatives for clinical use in the treatment of heart failure and sudden cardiac death. S.E.L. and S.R. are consultants for ARMGO Pharma, Inc.

Abbreviations: AFC, after-contraction; CL, cycle length; CPVT, catecholaminergic polymorphic VT; DAD, delayed after-depolarization; ISO, isoproterenol; I_{TI}, transient inward current; MAP, monophasic action potential; nsVT, nonsustained VT; PES, programmed electrical stimulation; RyR2, cardiac Ca^{2+} release channel/ryanodine receptor; SR, sarcoplasmic reticulum; sVT, sustained VT; VT, ventricular tachycardia.

‖To whom correspondence should be addressed. E-mail: arm42@columbia.edu.

www.pnas.org/cgi/doi/10.1073/pnas.0602133103

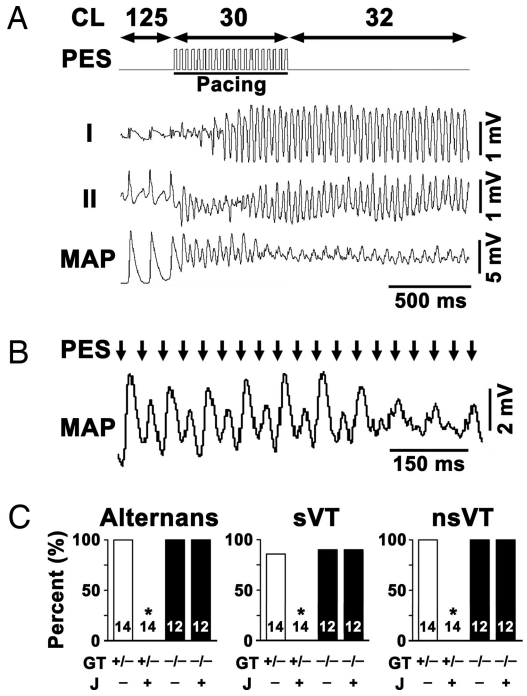

Fig. 1. Calstabin-2 deficiency causes pacing-induced bidirectional VT and MAP alternans, which are prevented by JTV519. (*A*) Representative lead I and II ECG tracings and simultaneous left ventricular epicardial MAP recording from a placebo-treated *calstabin-2*$^{+/-}$ mouse during overdrive pacing at CL 30 ms as documented by PES trace. Pacing triggered sustained bidirectional VT, as evidenced by simultaneous ECG and MAP recordings shown at higher resolution in *B*. Pacing stimuli (arrows) induced MAP alternans that continued after cessation of pacing in placebo-treated *calstabin-2*$^{+/-}$ mice (CL 32 ms). (*C*) Bar graphs summarizing simultaneous occurrence of bidirectional MAP alternans (*Left*) and sustained VT (sVT) (*Center*) or nonsustained VT (nsVT) (*Right*) arrhythmias in placebo-treated (J−) or JTV519-treated (J+) *calstabin-2*$^{+/-}$ (open bars) or *calstabin-2*$^{-/-}$ (filled bars) mice during ISO stimulation (0.5 mg·kg^{-1} body weight). Mouse numbers and dimensions are as indicated. sVT, >10 beats (*Center*); nsVT, 3–10 arrhythmogenic beats (*Right*). GT, genotype.

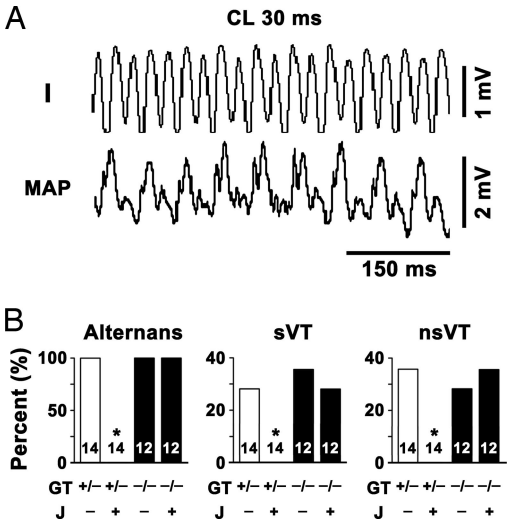

Fig. 2. Spontaneous bidirectional VT and MAP alternans in a *calstabin-2*$^{+/-}$ mouse (no pacing). (*A*) Simultaneous, representative ECG lead I tracing and left ventricular epicardial MAP recording from a placebo-treated *calstabin-2*$^{+/-}$ mouse during early phase of sVT. CL, cycle length. Bidirectional ECG QRS alternans and MAP alternans are closely correlated. (*B*) Bar graphs summarizing alternans (*Left*), sVTs (*Center*), or nsVTs (*Right*) in placebo-treated (J−) or JTV519-treated (J+) *calstabin-2*$^{+/-}$ (open bars) or *calstabin-2*$^{-/-}$ (filled bars) mice during ISO stimulation. GT, genotype.

treated conscious *calstabin-2*$^{+/-}$ and *calstabin-2*$^{-/-}$ mice revealed no significant differences in resting electrocardiographic parameters, including heart rate (RR interval) and conduction (PR, QRS, and rate-corrected QT interval), as reported in ref. 16. However, PES reproducibly induced bidirectional VT in *calstabin-2*$^{+/-}$ mice but not in WT controls (Fig. 1 *A* and *C*). Simultaneous epicardial monophasic action potential (MAP) recordings showed that PES-induced sustained or nonsustained VT (sVT or nsVT, respectively) correlated closely with MAP instability (Fig. 1 *A* and *B*). After ISO treatment, pacing at short cycle lengths (CLs) or premature coupling intervals (S1–S2; S1–S2–S3) resulted in MAP alternans, which continued after pacing stopped (Fig. 1*B*). Sustained MAP alternans occurred in 100% of sVT in *calstabin-2*$^{+/-}$ and *calstabin-2*$^{-/-}$ mice but never in WT controls (Fig. 1*C*). Sustained VT was observed in 86% of the *calstabin-2*$^{+/-}$ mice, which was not significantly different from *calstabin-2*$^{-/-}$ knockout mice (Fig. 1*C*); however, sVT was never observed in WT mice, confirming earlier results (7, 16).

Calstabin-2$^{+/-}$ mice pretreated for 1 week with JTV519 (0.5 mg·kg^{-1}·hr^{-1}) developed significantly fewer exercise-induced arrhythmias ($P < 0.05$) (Fig. 1*C*). In contrast, JTV519 caused no significant reduction of arrhythmias in *calstabin-2*$^{-/-}$-deficient mice, indicating that calstabin-2 is required for the antiarrhythmic actions of JTV519 (Fig. 1*C*). JTV519-treated *calstabin-2*$^{+/-}$ mice exhibited no sustained MAP alternans (Fig. 1*C*), indicating that JTV519 effectively increased the threshold for arrhythmia inducibility and MAP alternans.

Arrhythmias and MAP alternans also occurred spontaneously in *calstabin-2*$^{+/-}$ and *calstabin-2*$^{-/-}$ mice, and were never observed in WT mice (Fig. 2). JTV519 inhibited the occurrence of spontaneous arrhythmias and MAP alternans only in *calstabin-2*$^{+/-}$ mice but not in *calstabin-2*$^{-/-}$ mice (Fig. 2*B*).

To further test the hypothesis that calstabin-2 deficiency promotes dynamic electrical tissue heterogeneity during β-AR stimulation, we positioned two MAP electrodes at a fixed distance of 4 mm apart on the left ventricular free wall. During sVT progression, *calstabin-2*$^{+/-}$ mice exhibited a phase reversal of MAP alternans in the absence of pacing (Fig. 3). Because the surface MAP traces reflect the integrated electrical activity of intramural and epicardial cells, 3D optical mapping would be necessary to further differentiate between arrhythmic mechanisms of focal DAD activation versus automatic focus or breakthrough of reentrant waves. However, studies using optical mapping techniques have shown that discordant action potential alternans representing significant electrical instability precedes ventricular fibrillation (22). The fact that we observed discordant MAP alternans in calstabin-2-deficient mice suggests that both spatial MAP heterogeneities and local MAP instabilities create a dynamic substrate for arrhythmias, none of which were

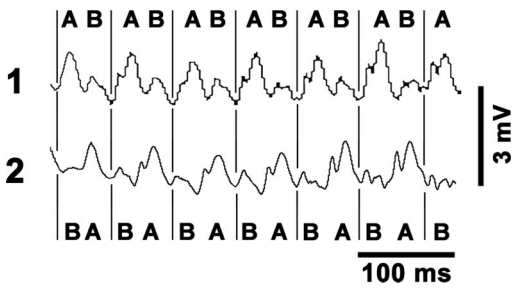

Fig. 3. Example of discordant MAP alternans in a haploinsufficient *calstabin-2*$^{+/-}$ mouse during pacing-induced sVT. Phase transition between epicardial MAP signal sites 1 and 2 is indicated by the letters ''A'' and ''B'' and by vertical lines.

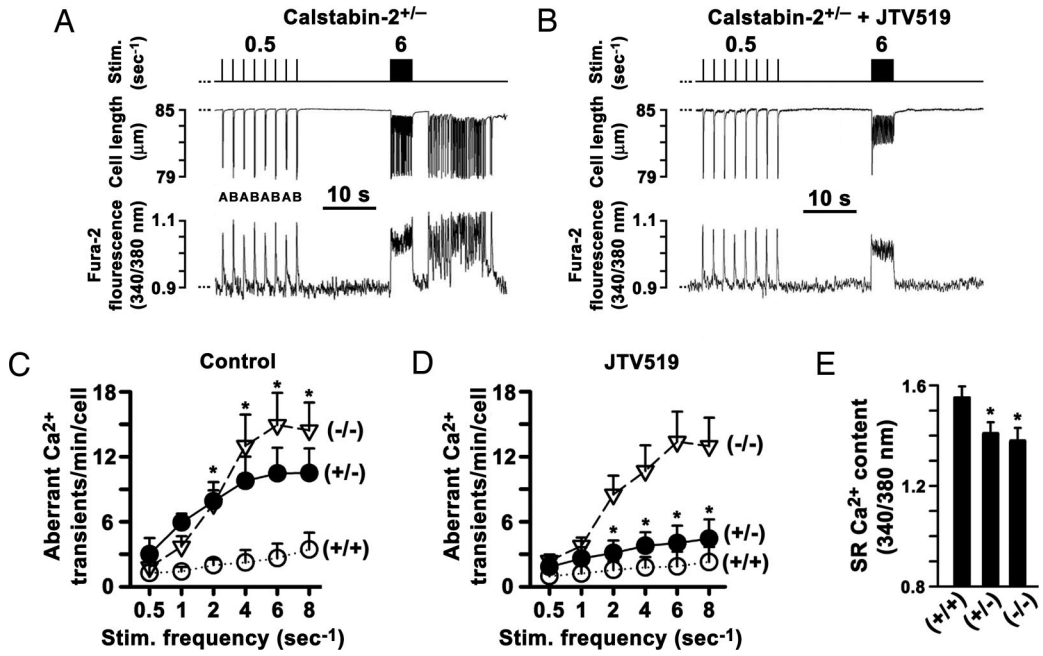

Fig. 4. Calstabin-2 deficiency causes aberrant diastolic Ca^{2+} release and after-contractions (AFCs) that are prevented by JTV519. (*A*) Alternating (indicated by ''A''/''B'') intracellular Ca^{2+} transients and AFCs in *calstabin-2*$^{+/-}$ cardiomyocyte paced at 0.5 Hz and aberrant Ca^{2+} release events after 6-Hz pacing. (*B*) JTV519 treatment prevented intracellular Ca^{2+} oscillations and AFCs in *calstabin-2*$^{+/-}$ cardiomyocytes after rapid pacing. (*C*) Ca^{2+} oscillations (min^{-1} $cell^{-1}$) are significantly increased at higher pacing rates in *calstabin-2*$^{+/-}$ or *calstabin-2*$^{-/-}$ cardiomyocytes compared with WT. (*D*) JTV519 treatment significantly decreased aberrant Ca^{2+} oscillations in heterozygous *calstabin-2*$^{+/-}$, but not *calstabin-2*$^{-/-}$, cardiomyocytes. (*E*) SR Ca^{2+} load measured by local caffeine application was significantly reduced in calstabin-2-deficient cardiomyocytes.

observed in WT mice or *calstabin-2*$^{+/-}$ mice after JTV519 treatment.

We examined *calstabin-2*$^{-/-}$-deficient cardiomyocytes paced by programmed field stimulation in the presence of 1 μM ISO. Each stimulation step between 0.5 and 8 s^{-1} was followed by a pause to monitor for aberrant intracellular Ca^{2+} release events and associated after-contractions (AFCs) (8). At 0.5 s^{-1} pacing frequency, aberrant Ca^{2+} release and AFCs were observed in <1% of WT, *calstabin-2*$^{+/-}$, or *calstabin-2*$^{-/-}$ cardiomyocytes in the presence of 1 μM ISO. Pacing at higher frequencies increased aberrant diastolic Ca^{2+} release and AFCs in 92% of *calstabin-2*$^{+/-}$ and in 95% of *calstabin-2*$^{-/-}$ cardiomyocytes at 6 s^{-1} (Fig. 4 *A* and *C*). Previously, we reported that rapid pacing combined with β-AR stimulation induced DADs in *calstabin-2*$^{-/-}$ cardiomyocytes (7). It is therefore likely that these DADs are triggered by aberrant intracellular Ca^{2+} release in the setting of β-AR stimulation and rapid pacing.

Preincubation of haploinsufficient *calstabin-2*$^{+/-}$ cardiomyocytes with 1 μM JTV519 significantly reduced the number of aberrant diastolic Ca^{2+} release events and AFCs after rapid pacing in *calstabin-2*$^{+/-}$, but not *calstabin-2*$^{-/-}$, knockout cardiomyocytes ($P < 0.05$) (Fig. 4 *B* and *D*). Application of caffeine indicated that SR Ca^{2+} store content was significantly reduced by 9 ± 0.3% or 10 ± 0.4% in ISO-treated *calstabin-2*$^{+/-}$ and *calstabin-2*$^{-/-}$ cardiomyocytes compared with WT (1-Hz preconditioning; $P < 0.05$) (Fig. 4*E*), indicating that calstabin-2 deficiency promotes a net SR Ca^{2+} leak during β-AR stimulation.

ISO treatment of isolated *calstabin-2*$^{+/-}$ cardiomyocytes for 30 min resulted in maximal RyR2 PKA phosphorylation in the presence of sodium fluoride (1 mM) and significant depletion of calstabin-2 from the RyR2 complex (Fig. 5*A*). JTV519 significantly increased calstabin-2 binding to PKA-phosphorylated RyR2 in *calstabin-2*$^{+/-}$ cardiomyocytes (Fig. 5*B*). We previously found that JTV519 treatment normalizes PKA-hyperphosphorylated RyR2 channel function *in vitro* and *in vivo* (1, 16, 17).

Diastolic SR Ca^{2+} release may activate a Ca^{2+}-dependent transient inward current (I_{TI}) that triggers DADs in *calstabin-2*$^{-/-}$ cardiomyocytes (7, 8). Using combined confocal Ca^{2+} imaging and patch-clamp (Fig. 6*A*), a depolarizing step after preconditioning and stimulation with 1 μM ISO revealed no

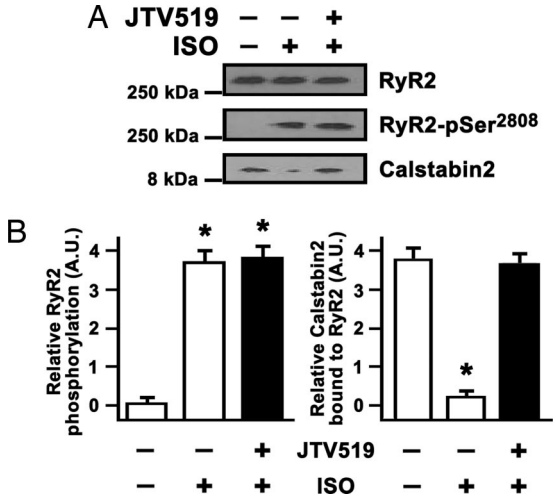

Fig. 5. JTV519 increased calstabin-2 binding to RyR2 in cardiomyocytes during β-AR stimulation. (*A*) RyR2 immunoprecipitation from *calstabin-2*$^{+/-}$ cardiomyocyte lysate demonstrating increased PKA phosphorylation of RyR2 at Ser-2808 and calstabin-2 depletion after a 30-min exposure to 100 nM isoproterenol (ISO). Pretreatment with 1 μM JTV519 prevented calstabin-2 release from RyR2 despite PKA Ser-2808 phosphorylation. (*B*) Bar graphs summarizing results from three myocyte isolations each assessed in triplicate. *, $P < 0.05$.

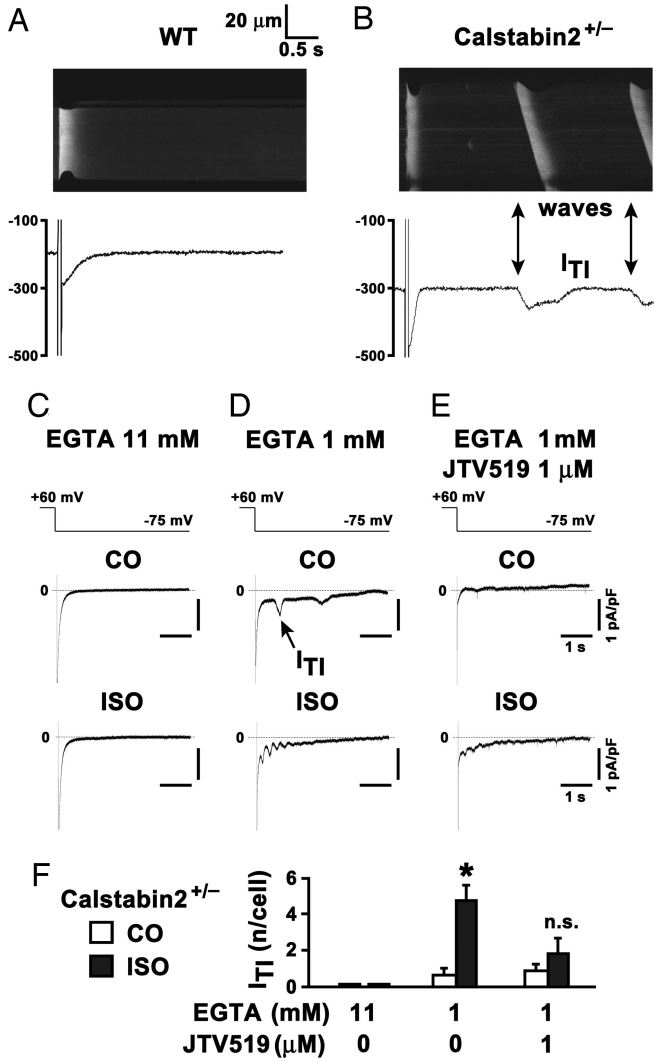

Fig. 6. Inhibition of calcium-dependent transient inward current (I_{TI}) in haploinsufficient *calstabin-2*$^{+/-}$ cardiomyocytes by JTV519. (*A*) Confocal Ca^{2+} line scan image of isolated WT cardiomyocyte current trace during 1 μM isoproterenol (ISO). After a depolarization–repolarization step, the I_{Ca} tail current rapidly activated a homogeneous intracellular $[Ca^{2+}]_i$ transient followed by a long electrically stable resting phase. (*B*) In contrast, in *calstabin-2*$^{+/-}$ cardiomyocytes, intracellular Ca^{2+} sparks and Ca^{2+} waves (arrows) were frequent, and Ca^{2+} waves coincide with I_{TI} (arrows) under the same conditions. Scales are the same as in *A*. (*C*) Typical current traces were recorded at −75 mV after a preconditioning depolarization train under control conditions (CO) or after 4 min of 1 μM ISO in cells dialyzed with 11 or 1 mM EGTA (*D*) or 1 mM EGTA and 1 μM JTV519 pretreatment (*E*). Scales in *C–E* are as indicated. (*F*) Bar graph summarizes average number of I_{TI}s per cell under indicated experimental conditions. No I_{TI} was detected in cells dialyzed with 11 mM EGTA ($n = 4$, each CO and ISO). In *calstabin-2*$^{+/-}$ cells dialyzed with 1 mm EGTA, ISO significantly increased the number of I_{TI}s per cell (CO, $n = 6$; ISO, $n = 5$; $P < 0.05$). The number of I_{TI}s in *calstabin-2*$^{+/-}$ cells treated with 1 μM JTV519 and dialyzed with 1 mM EGTA was not significantly increased by ISO (CO, $n = 7$; ISO, $n = 11$).

aberrant Ca^{2+} release events in WT cardiomyocytes. However, repeating the same protocol during ISO stimulation in *calstabin-2*$^{+/-}$ cardiomyocytes promoted Ca^{2+} sparks and Ca^{2+} waves (Fig. 6*B*), which coincided with the depolarizing I_{TI} and thus are a potential source of DADs and electrical instability (8).

After rapid pacing at 10 s^{-1}, plasma membrane current traces from isolated *calstabin-2*$^{+/-}$ cardiomyocytes dialyzed with 11 mM EGTA to clamp intracellular $[Ca^{2+}]_i$ at low concentrations showed no I_{TI} before or 4 min after 1 μM ISO treatment (Fig. 6*C*). However, *calstabin-2*$^{+/-}$ cardiomyocytes dialyzed with 1 mM EGTA to clamp $[Ca^{2+}]_i$ at ≈100 nM, which is characteristic for resting cells in diastole, exhibited a low number of I_{TI} events after pacing that were greater than ≈5-fold increased by ISO treatment ($P < 0.05$) (Fig. 6*D*). When the identical protocol was repeated in cardiomyocytes pretreated with 1 μM JTV519 and dialyzed with 1 mM EGTA, I_{TI}s were inhibited (Fig. 6 *E* and *F*). Thus, either $[Ca^{2+}]_i$ clamp with 11 mM EGTA or JTV519 treatment resulted in significant inhibition of I_{TI}s (Fig. 6*F*)

Discussion

In the present study we have shown that calstabin-2 deficiency is associated with aberrant SR Ca^{2+} release, Ca^{2+}-dependent I_{TI}s, MAP alternans, and bidirectional VTs, all of which can be prevented by JTV519.

Our study extends earlier reports showing that intracellular $[Ca^{2+}]_i$ alternans (Fig. 4*A*) gives rise to action potential alternans at the *in vivo* level (23, 24). We have documented diastolic SR Ca^{2+} leak induced by rapid pacing and β-AR stimulation in *calstabin-2*$^{+/-}$ mice as a mechanism of MAP alternans and bidirectional VT. Spatially discordant MAP alternans was observed during sustained arrhythmias in *calstabin-2*$^{+/-}$ mice, suggesting diastolic SR Ca^{2+} leak as a mechanism underlying electrical tissue heterogeneity, as described previously by using optical mapping (22). SR Ca^{2+} wave fronts in *calstabin-2*$^{+/-}$ cardiomyocytes consistently activated I_{TI} as a source of electrical membrane instability.

In ISO-treated *calstabin-2*$^{+/-}$ cardiomyocytes, aberrant diastolic SR Ca^{2+} release correlated closely with the pacing frequency (Fig. 4*C*). Earlier studies showed a relationship between plasma membrane action potential oscillations and $[Ca^{2+}]_i$ alternans (23, 24).

Because six distinct CPVT-linked RyR2 mutations exhibited significantly reduced calstabin-2 binding to RyR2 (1, 7), *calstabin-2*$^{+/-}$ cardiomyocytes may represent a model for CPVT. Indeed, the RyR2-R4496C knockin CPVT mouse (25) shows a similar phenotype to that observed in *calstabin-2*$^{+/-}$ mice, catecholaminergic bidirectional VT. Because the bidirectional VT in the *calstabin-2*$^{+/-}$ mice was closely associated with MAP alternans throughout the arrhythmia, it seems likely that the alternating bidirectional ECG pattern observed in CPVT is directly related to MAP and $[Ca^{2+}]_i$ alternans. Importantly, enhanced calstabin-2 binding to PKA-phosphorylated RyR2 prevented MAP alternans, I_{TI}s, and arrhythmias only in *calstabin-2*$^{+/-}$ mice, further implicating calstabin-2 depletion and diastolic SR Ca^{2+} leak as key antiarrhythmic targets (16).

Treatment of calstabin-2$^{+/-}$ mice with JTV519 suppressed MAP alternans and cellular I_{TI}s, preventing initiation of ventricular arrhythmias during all pacing protocols. These data indicate that MAP alternans and (as previously shown) DADs in *calstabin-2*$^{-/-}$ cardiomyocytes (7) may induce propagation of arrhythmic excitation waves. Inhibition of RyR2-mediated diastolic SR Ca^{2+} leak by JTV519 represents a previously unrecognized treatment opportunity for prevention of sudden cardiac death in patients with CPVT and heart failure.

Materials and Methods

Animal Preparation. Studies were carried out according to the National Institutes of Health guidelines and approved by the institutional animal care and use committee.

***In Vivo* Electrophysiology.** Subcutaneous six-lead ECG recordings were obtained (model VR12; Electronics for Medicine, Pleasantville, NY). An MAP contact electrode was gently placed on the left ventricular anterior free wall by using a 3D micromanipulator and digitized MAP recording was used to monitor changes in epicardial membrane potential as described in ref. 26.

PHYSIOLOGY

A small platinum electrode was placed on the right ventricular free wall for PES. Pacing (S1–S2) at CLs between 70 and 200 ms, interpolating a single premature stimulus every 10 beats, was performed to determine effective refractory period at twice diastolic threshold strength. Rapid pacing was increased until 2:1 block. In a subset of mice, two MAP electrodes were gently placed on the left anterior free wall during sustained VTs. Animals were treated with either JTV519 (7-day continuous infusion 0.5 $mg \cdot kg^{-1} \cdot hr^{-1}$) or placebo (carrier). ISO was administered by i.p. injection (0.5 $mg \cdot kg^{-1}$) (16). CL was averaged from 10 consecutive RR intervals.

Cell Isolation. Cardiomyocytes from WT, *calstabin-2*$^{+/-}$, or *calstabin-2*$^{-/-}$ mice were enzymatically dissociated and isolated as described in ref. 27. Extracellular Ca^{2+} was sequentially increased, and the final solution consisted of 2.5 mM $CaCl_2$, 137 mM NaCl, 5.4 mM KCl, 1.0 mM MgCl, 0.33 mM NaH_2PO_4, 10 mM Hepes, and 10 mM glucose (pH 7.4).

Intracellular Ca^{2+} Imaging. Cardiomyocytes were incubated in a 10 μM solution of fura-2 acetoxymethylester ester (Molecular Probes) for 10 min at room temperature, followed by resuspension in fura-2-free solution for 30 min. Cells were plated in a perfusion chamber placed on the stage of an inverted microscope coupled to a video camera and a microfluorometry system. Cell length was monitored with a video-edge detector. For intracellular $[Ca^{2+}]_i$ measurements, fura-2 fluorescence was measured by using a photomultiplier (DeltaRam; PTI, South Brunswick, NJ). The ratio of emitted fluorescence at 340 and 380 nm was converted to $[Ca^{2+}]_i$. Cardiomyocytes were field-stimulated with 3-ms pulses at increasing frequencies (0.5–8 s^{-1}) by programmed field stimulation (ALA Scientific Instruments, Westbury, NY) in the presence of 100 nM ISO at 37°C. Cardiomyocytes were pretreated with 1 μM JTV519 or the carrier solution (0.1% DMSO) for 2 h. In a subgroup of cells, after stabilization of twitch and Ca^{2+} transient amplitude, stimulation was stopped, and SR Ca^{2+} load was measured by rapid caffeine application (10 mM) by using a local perfusion system (Warner Instruments, Hamden, CT). After $[Ca^{2+}]_i$ decline and caffeine washout, a second caffeine application was applied to confirm complete SR Ca^{2+} release.

Electrophysiology. Cardiomyocytes were placed in a Petri dish on the stage of an inverted microscope, and whole-cell patch-clamp was performed at 22°C. The control solution contained 132 mM NaCl, 4.8 mM KCl, 10 mM Hepes, 5 mM glucose, 2 mM $CaCl_2$, and 1.2 mM $MgCl_2$ (pH 7.4). Two different pipette solutions were used: 110 mM K-aspartate, 5 mM ATP-K_2, 10 mM Hepes, 1 mM $MgCl_2$, 0.5 mM $CaCl_2$, and 1 mM EGTA (or 5.5 mM $CaCl_2$ and 11 mM EGTA) (pH 7.3). For both pipette solutions, the concentration of free calcium was set at 100 nM, corresponding to diastole. Currents were recorded in response to a stimulation protocol consisting of a preconditioning train of 30 depolarizing steps to +60 mV (50-ms duration) from a holding potential of −75 mV at 10 Hz, followed by a 500-ms pause at −75 mV, after which a single depolarization to +60 mV was elicited, followed by a 4-s recording interval at −75 mV. The same protocol was applied in control solution and in the presence of 1 μM ISO. Data were acquired by using PCLAMP 8.0 software (Axon Instruments, Union City, CA) and analyzed with ORIGIN 7.0 software (OriginLab, Northampton, MA) and CLAMPFIT 8.2 (Axon Instruments).

Simultaneous Recording of I_{Ti}s and Confocal Imaging of Ca^{2+} Sparks and Ca^{2+} Waves. To simultaneously measure I_{Ca}-induced Ca^{2+} release from the SR, fluo-4 was excited at 488 nm, and the fluorescence was detected at 510 nm with a laser scanning confocal microscope (LSM 510; Zeiss). Cell capacitance and I_{Ca} density were calculated with CLAMPEX 9.0 (Axon Instruments). Global Ca^{2+} release was analyzed by routines compiled with IDL 6.0 (Research Systems, Boulder, CO). Myocytes were incubated with fluo-4 acetoxymethylester (10 μM) and, after a 20-min period, were superfused with an extracellular solution containing 1.8 mM Ca^{2+}. Cells were field-stimulated at 1.0 Hz to produce steady-state conditions. Within the first 10 s after the last depolarization of a 15-pulse train, spontaneous nonpropagating Ca^{2+} release was recorded for the next three to four image frames at high resolution (800 lines per frame, 1.92 ms per line) and identified as "diastolic Ca^{2+} sparks." The recording sequence was repeated three times in each cell. Line-scan images were analyzed and Ca^{2+} sparks were detected offline with a computer-based detection algorithm.

Data Analysis. Data are expressed as average ± SEM. ANOVA with repeated measures was used for comparison between different groups, and Student's *t* test was used for comparison between groups. $P < 0.05$ was accepted as significant.

1. Lehnart, S. E., Wehrens, X. H., Laitinen, P. J., Reiken, S. R., Deng, S. X., Cheng, Z., Landry, D. W., Kontula, K., Swan, H. & Marks, A. R. (2004) *Circulation* **109,** 3208–3214.
2. Laitinen, P. J., Brown, K. M., Piippo, K., Swan, H., Devaney, J. M., Brahmbhatt, B., Donarum, E. A., Marino, M., Tiso, N., Viitasalo, M., *et al.* (2001) *Circulation* **103,** 485–490.
3. Priori, S. G., Napolitano, C., Tiso, N., Memmi, M., Vignati, G., Bloise, R., Sorrentino, V. & Danieli, G. A. (2001) *Circulation* **103,** 196–200.
4. De Rosa, G., Delogu, A. B., Piastra, M., Chiaretti, A., Bloise, R. & Priori, S. G. (2004) *Pediatr. Emerg. Care* **20,** 175–177.
5. George, C. H., Higgs, G. V. & Lai, F. A. (2003) *Circ. Res.* **93,** 531–540.
6. Li, Y., Kranias, E. G., Mignery, G. A. & Bers, D. M. (2002) *Circ. Res.* **90,** 309–316.
7. Wehrens, X. H., Lehnart, S. E., Huang, F., Vest, J. A., Reiken, S. R., Mohler, P. J., Sun, J., Guatimosim, S., Song, L. S., Rosemblit, N., *et al.* (2003) *Cell* **113,** 829–840.
8. Berlin, J. R., Cannell, M. B. & Lederer, W. J. (1989) *Circ. Res.* **65,** 115–126.
9. Johnson, N., Danilo, P., Jr., Wit, A. L. & Rosen, M. R. (1986) *Circulation* **74,** 1168–1179.
10. Priori, S. G. & Corr, P. B. (1990) *Am. J. Physiol.* **258,** H1796–H1805.
11. Kieval, R. S., Butler, V. P., Jr., Derguini, F., Bruening, R. C. & Rosen, M. R. (1988) *J. Am. Coll. Cardiol.* **11,** 637–643.
12. Marx, S. O., Reiken, S., Hisamatsu, Y., Jayaraman, T., Burkhoff, D., Rosemblit, N. & Marks, A. R. (2000) *Cell* **101,** 365–376.
13. Wehrens, X. H., Lehnart, S. E., Reiken, S. R. & Marks, A. R. (2004) *Circ. Res.* **94,** e61–e70.
14. Yano, M., Ono, K., Ohkusa, T., Suetsugu, M., Kohno, M., Hisaoka, T., Kobayashi, S., Hisamatsu, Y., Yamamoto, T., Noguchi, N., *et al.* (2000) *Circulation* **102,** 2131–2136.
15. Huang, F., Shan, J., Reiken, S., Wehrens, X. H. & Marks, A. R. (2006) *Proc. Natl. Acad. Sci. USA* **103,** 3456–3461.
16. Wehrens, X. H., Lehnart, S. E., Reiken, S. R., Deng, S. X., Vest, J. A., Cervantes, D., Coromilas, J., Landry, D. W. & Marks, A. R. (2004) *Science* **304,** 292–296.
17. Wehrens, X. H., Lehnart, S. E., Reiken, S., van der Nagel, R., Morales, R., Sun, J., Cheng, Z., Deng, S. X., de Windt, L. J., Landry, D. W. & Marks, A. R. (2005) *Proc. Natl. Acad. Sci. USA* **102,** 9607–9612.
18. Shannon, T. R., Pogwizd, S. M. & Bers, D. M. (2003) *Circ. Res.* **93,** 592–594.
19. Pogwizd, S. M. (1995) *Circulation* **92,** 1034–1048.
20. Pogwizd, S. M., Hoyt, R. H., Saffitz, J. E., Corr, P. B., Cox, J. L. & Cain, M. E. (1992) *Circulation* **86,** 1872–1887.
21. Pogwizd, S. M. & Corr, P. B. (1987) *Circ. Res.* **61,** 352–371.
22. Laurita, K. R., Girouard, S. D. & Rosenbaum, D. S. (1996) *Circ. Res.* **79,** 493–503.
23. Goldhaber, J. I., Xie, L. H., Duong, T., Motter, C., Khuu, K. & Weiss, J. N. (2005) *Circ. Res.* **96,** 459–466.
24. Chudin, E., Goldhaber, J., Garfinkel, A., Weiss, J. & Kogan, B. (1999) *Biophys. J.* **77,** 2930–2941.
25. Cerrone, M., Colombi, B., Santoro, M., di Barletta, M. R., Scelsi, M., Villani, L., Napolitano, C. & Priori, S. G. (2005) *Circ. Res.* **96,** e77–e82.
26. Chiello Tracy, C., Cabo, C., Coromilas, J., Kurokawa, J., Kass, R. S. & Wit, A. L. (2003) *Am. J. Physiol.* **284,** H168–H175.
27. Lehnart, S. E., Wehrens, X. H., Reiken, S., Warrier, S., Belevych, A. E., Harvey, R. D., Richter, W., Jin, S. L., Conti, M. & Marks, A. R. (2005) *Cell* **123,** 25–35.